Journal of Molecular Structure 1094 (2015) 137–147

Contents lists available at ScienceDirect

Journal of Molecular Structure

journal homepage: www.elsevier.com/locate/molstruc

Structural investigations of a series of 1,6-aryl-7-hydroxy-2,3-dihydroimidazo[1,2-*a*]pyrimidin-5(1*H*)-ones with potential antinociceptive activity

Waldemar Wysocki [a], Zbigniew Karczmarzyk [a,*], Marzena Rządkowska [b], Elżbieta Szacoń [b], Dariusz Matosiuk [b], Zofia Urbańczyk-Lipkowska [c], Przemysław Kalicki [c]

[a] Department of Chemistry, Siedlce University of Natural Sciences and Humanities, 3 Maja 54, 08-110 Siedlce, Poland
[b] Department of Synthesis and Chemical Technology of Pharmaceutical Substances, Medical University, Chodźki 4A, 20-093 Lublin, Poland
[c] Institute of Organic Chemistry, Polish Academy of Sciences, Kasprzaka 44/52, 01-224 Warszawa 42, Poland

HIGHLIGHTS

- Structural analysis of new bioactive imidazo[1,2-*a*]pyrimidines were undertaken.
- All compounds were characterized by IR, ^{1}H and ^{13}C NMR, X-ray and DFT methods.
- Keto–enol tautomeric equilibrium were investigated using DFT method.

GRAPHICAL ABSTRACT

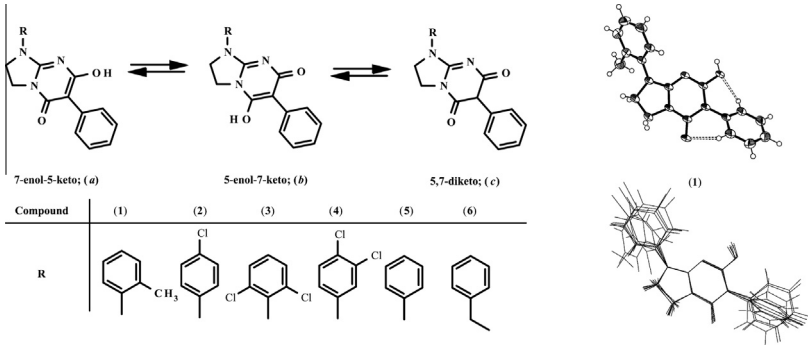

ARTICLE INFO

Article history:
Received 11 December 2014
Received in revised form 6 March 2015
Accepted 6 April 2015
Available online 11 April 2015

Keywords:
Imidazo[1,2-*a*]pyrimidine derivatives
Keto–enol tautomerism
X-ray structure
DFT calculations
Correlation analysis

ABSTRACT

The structural investigations of a series of new bioactive imidazo[1,2-*a*]pyrimidines **1**–**6** were undertaken using IR, ^{1}H and ^{13}C NMR spectroscopic analysis, X-ray crystal structure determinations and theoretical calculations. The compounds **1**–**6** were obtained by condensation of the respective 1-aryl-4,5-dihydro-1*H*-imidazol-2-amine hydrobromide and diethyl phenylmalonate in presence of sodium methoxide in methanol and for these compounds the equilibrium between possible O10-enol/O11-keto (***a***), O11-enol/O10-keto (***b***) and O10,O11-diketo (***c***) tautomeric forms were investigated in the gaseous phase, solution and crystalline state. Spectroscopic studies ^{1}H, ^{13}C NMR and IR allowed for the identification of the compounds **1**–**6** but they did not indicate explicitly their tautomeric forms present in solution and in the solid state. The X-ray analysis showed that the molecules of all investigated compounds exist as the O10-enol/O11-keto (***a***) tautomeric form in the crystalline state. The hydroxyl and carbonyl groups characteristic for existing tautomeric form are involved in a strong intra- and/or intermolecular O—H···O and O—H···N hydrogen bonds. The theoretical calculations at DFT/B3LYP/6-311++G(d,p) level showed that two tautomeric forms (***a***) and (***c***) can coexist both in gas phase and the solution with the population of them being in the relation (***a***) > (or ≫) (***c***). The comparison of the experimentally recorded IR, ^{1}H and ^{13}C spectra with the corresponding spectra theoretically calculated for all possible tautomeric forms of **1**–**6** shows that the correlation of experimental and theoretical spectra can be used to a limited extent for the identification of tautomeric forms.

* Corresponding author. Tel.: +48 25 643 1017; fax: +48 25 644 20 45.
E-mail address: kar@uph.edu.pl (Z. Karczmarzyk).

http://dx.doi.org/10.1016/j.molstruc.2015.04.005
0022-2860/

Introduction

Both synthetic and natural compounds containing imidazo[1,2-*a*]pyrimidine system exhibit wide spectrum of biological activity such as anticonvulsant and tranquilizer [1], antineoplastic [2], anti-inflammatory [3,4] and antimicrobial [5]. Dioxo derivatives of fused imidazoline ring systems, *e.g.* imidazo[1,2-*a*]imidazoles, imidazo[1,2-*a*][1,3,5]triazines and imidazo[2,1-*c*][1,2,4]triazines, were found to have significant analgesic opioid-like action but without the typical narcotic side-effects [6,7]. Modification of their structure led us to the synthesis a series of 1-aryl-6-phenyl-5,7-dioxo-imidazo[1,2-*a*]pyrimidines **1**–**6** (Scheme 1), which in the pharmacological tests show antinociceptive and serotonergic activity in CNS system with an average or low acute toxicity. One of the method to synthesize these compounds is condensation of respective 1-aryl-4,5-dihydro-1*H*-imidazol-2-amine hydrobromide, diethyl phenylmalonate in alkaline media [8]. Obtained derivatives can exist in 7-enol–5-keto (***a***), 5-enol–7-keto (***b***) and 5,7-diketo (***c***) tautomeric forms (Scheme 1).

In order to determine the keto–enol tautomeric equilibrium within a series of imidazo[1,2-*a*]pyrimidines **1**–**6**, IR, ^{1}H and ^{13}C NMR spectroscopic analysis, X-ray crystal structure determinations and theoretical calculations were undertaken for all **1**–**6** investigated compounds. The tautomerism of the oxo groups would be responsible for the selectivity of action, as we have already confirmed for structurally related imidazo[2,1-*c*][1,2,4] triazines [9]. We report here the structural characterization of compounds **1**–**6** in terms of their tautomeric equilibrium in crystalline state, in solution and in gaseous phase.

Experimental

General methods

The ^{1}H and ^{13}C NMR spectra were recorded at room temperature on a Varian 400-MR spectrometer at 399.67 and 100.50 MHz, respectively. Chemical shift (δ) are given in ppm, referenced to the residual proton (2.50 ppm) and carbon (39.51 ppm) resonance of the DMSO-d_6. IR spectra were recorded on a FTIR MAGNA-IR 760 Nicolet spectrometer for **1**–**6** in the solid state (KBr) and for **4** in chloroform ($CHCl_3$).

*Synthesis of compounds **1**–**6** [8]*

The mixture of respective 1-aryl-2-aminoimidazoline hydrobromide (0.02 mol), diethyl phenylmalonate (0.02 mol), 15 ml of 16.7% solution of sodium methoxide in methanol (60 ml) were refluxed for 3 h. The solvent was evaporated. After cooling the crude product was dissolved in water and neutralized with 10% solution of hydrochloric acid. The solid product was filtrated off and recrystallized from propan-2-ol.

*Spectroscopic data of compounds **1**–**6***

*7-Hydroxy-1-(2-methylphenyl)-6-phenyl-2,3-dihydroimidazo[1,2-a]pyrimidin-5(1H)-one (**1**)*

^{1}H NMR: (400 MHz, DMSO-d_6, ppm) δ = 10.90 (s, 1H, OH), 7.45 (m, 1H, CH), 7.40 (m, 2H, 2 × CH), 7.30 (m, 5H, 5 × CH), 7.12 (t, 1H, CH, J = 7.2 Hz), 4.15 (t, 2H, CH_2, J = 9.2 Hz), 4.01 (t, 2H, CH_2, J = 9.2 Hz), 2.30 (s, 3H, CH_3);

^{13}C NMR: (100 MHz, DMSO-d_6, ppm) δ = 166.9 (C═O), 161.2 (C—OH), 153.5 (C═N), Ar (CH): 136.9, 136.5, 134.0, 131.0, 130.6, 128.2, 127.8, 127.1, 127.0, 125.1, 93.3, (C═CO), 47.9 (CH_2), 41.1 (CH_2), 17.5 (CH_3);

IR: (KBr, cm^{-1}) ν = 3171 (OH), 1640 (C═O), 1606, 1566, 1504, 1409, 1316, 1213, 1175, 1126, 1099, 767, 737, 701, 587, 458.

*1-(4-Chlorphenyl)-7-hydroxy-6-phenyl-2,3-dihydroimidazo[1,2-a]pyrimidin-5(1H)-one (**2**)*

^{1}H NMR: (400 MHz, DMSO-d_6, ppm) δ = 11.05 (s, H, OH), 7.90 (m, 2H, 2 × CH), 7.45 (m, 4H, 4 × CH), 7.43 (m, 2H, 2 × CH), 7.16 (m, 1H, CH), 4.11 (m, 4H, 2 × CH_2);

^{13}C NMR: (100 MHz, DMSO-d_6, ppm) δ = 165.9 (C═O), 160.9 (C—OH), 151.2 (C═N), Ar (CH): 138.1, 133.5, 130.5, 128.6, 127.1, 127.0, 125.4, 120.2, 94.7 (C═CO), 45.1 (CH_2), 40.0 (CH_2);

IR: (KBr, cm^{-1}) ν = 3431 (OH), 3068, 2958, 2914, 2868, 1735, 1660 (C═O), 1600, 1552, 1503, 1401, 1257, 1233, 1006, 826, 716, 534, 512.

*1-(2,6-Dichlorphenyl)-7-hydroxy-6-phenyl-2,3-dihydroimidazo[1,2-a]pyrimidin-5(1H)-one (**3**)*

^{1}H NMR: (400 MHz, DMSO-d_6, ppm) δ = 11.08 (s, 1H, OH), 7.67 (d, 2H, 2 × CH, J = 8.0 Hz), 7.51 (t, 1H, CH, J = 8.0 Hz), 7.39 (d, 2H, 2 × CH, J = 7.2 Hz), 7.26 (t, 2H, 2 × CH, J = 8.0 Hz), 7.13 (t, 1H, CH, J = 7.2 Hz), 4.26 (t, 2H, CH_2, J = 8.8 Hz), 4.01 (t, 2H, CH_2, J = 8.8 Hz);

^{13}C NMR: (100 MHz, DMSO-d_6, ppm) δ = 166.9 (C═O), 160.9 (C—OH), 153.0 (C═N), Ar (CH): 135.4, 133.6, 132.3, 131.5, 130.6, 129.3, 127.0, 125.3, 94.0 (C═CO), 45.4 (CH_2), 41.5 (CH_2);

IR: (KBr, cm^{-1}) ν = 3435 (OH), 2899, 2637, 1668 (C═O), 1557, 1423, 1341, 1308, 1247, 1182, 1092, 849, 784, 741, 698, 592, 536, 450.

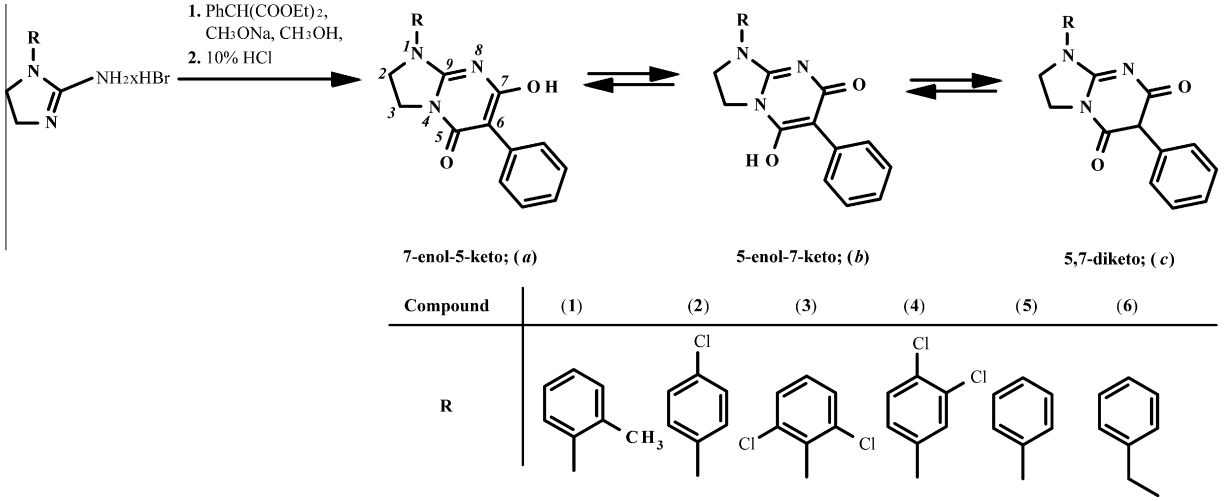

Scheme 1.

*1-(3,4-Dichlorphenyl)-7-hydroxy-6-phenyl-2,3-dihydroimidazo[1,2-a]pyrimidin-5(1H)-one (**4**)*

^{1}H NMR: (400 MHz, DMSO-d_6, ppm) δ = 11.22 (s, 1H, OH), 8.29 (d, 1H, CH, J = 2.4 Hz), 7.77 (dd, 1H, CH, J = 8.8, J = 2.8 Hz), 7.64 (d, 1H, CH, J = 9.2 Hz), 7.45 (m, 2H, 2 × CH), 7.28 (t, 2H, CH, J = 7.2 Hz), 7.16 (m, 1H, CH), 4.11 (m, 4H, 2 × CH_2);

^{13}C NMR: (100 MHz, DMSO-d_6, ppm) δ = 165.8 (C═O), 160.8 (C—OH), 150.9 (C═N), Ar (CH): 139.2, 133.4, 131.3, 130.5, 130.4, 127.1, 125.5, 124.6, 119.8, 118.2, 95.0 (C═CO), 45.1 (CH_2), 40.1 (CH_2);

IR: (KBr, cm^{-1}) ν = 3434 (OH), 3032, 2654, 1637 (C═O), 1541, 1509, 1416, 1385, 1332, 1274, 1238, 1185, 1136, 1114, 1042, 791, 705, 592, 494;

IR: ($CHCl_3$, cm^{-1}) ν = 3072, 3028, 2927, 2854, 1659 (C═O), 1551, 1482, 1308, 1178, 795, 787, 701, 693, 678, 667.

*7-Hydroxy-1,6-diphenyl-2,3-dihydroimidazo[1,2-a]pyrimidin-5(1H)-one (**5**)*

^{1}H NMR: (400 MHz, DMSO-d_6, ppm) δ = 10.98 (s, 1H, OH), 7.85 (m, 2H, 2 × CH), 7.43 (m, 4H, 4 × CH), 7.29 (m, 2H, 2 × CH), 7.16 (m, 2H, 2 × CH), 4.14 (m, 4H, 2 × CH_2);

^{13}C NMR: (100 MHz, DMSO-d_6, ppm) δ = 166.0 (C═O), 160.9 (C—OH), 151.4 (C═N), Ar (CH): 133.7, 130.5, 128.8, 127.1, 125.3, 123.4, 119.0, 94.3 (C═CO), 45.2 (CH_2), 40.1 (CH_2);

IR: (KBr, cm^{-1}) ν = 3430 (OH), 2905, 1632 (C═O), 1591, 1545, 1509, 1493, 1405, 1317, 1244, 1177, 790, 760, 583, 516.

*1-Benzyl-7-hydroxy-6-phenyl-2,3-dihydroimidazo[1,2-a]pyrimidin-5(1H)-one (**6**)*

^{1}H NMR: (400 MHz, DMSO-d_6, ppm) δ = 10.90 (s, 1H, OH), 7.36 (m, 7H, 7 × CH), 7.28 (t, 2H, 2 × CH), 7.11 (t, 1H, 1 × CH), 4.58 (s, 2H, 1 × CH_2), 3.97 (t, 2H, 1 × CH_2), 3.57 (t, 2H, 1 × CH_2);

^{13}C NMR: (100 MHz, DMSO-d_6, ppm) δ = 167.2 (C═O), 161.6 (C—OH), 154.8 (C═N), Ar (CH): 136.1, 130.6, 128.7, 127.7, 127.5, 127.0, 126.6, 124.9, 83.3 (C═CO), 47.3 (CH_2), 44.3 (CH_2), 40.7 (CH_2);

IR: (KBr, cm^{-1}) ν = 3435 (OH), 3048, 1652 (C═O), 1606, 1551, 1417, 1359, 1298, 1172, 1081, 989, 860, 780, 740, 703, 582, 495, 459.

X-ray structure analysis

Colorless prismatic crystals of **1**–**3** suitable for X-ray diffraction analysis were grown by slow evaporation of a methanol solution, while the needle crystals of **4** were obtained from DMSO and prismatic crystals of **5** and **6** were crystallized from propan-1-ol. X-ray data of **1**–**3** were collected on the Kuma KM-4 four-circle diffractometer at room temperature; crystal sizes: 0.60 × 0.40 × 0.30 mm (**1**), 0.50 × 0.30 × 0.20 mm (**2**) and 0.20 × 0.20 × 0.10 mm (**3**); Cu Kα (λ = 1.54178 Å) radiation, ω–2θ scans. Data collections for **4**, **5** and **6** were performed on the Bruker SMART APEX II CCD diffractometer at room temperature; crystal sizes 0.28 × 0.19 × 0.14 mm (**4**), 0.28 × 012 × 0.02 mm (**5**) and 0.59 × 0.17 × 0.07 mm (**6**), Cu Kα (λ = 1.54178 Å) radiation, φ and ω scans. The structures were solved by direct methods using

Table 1
Crystal data and structure refinement for **1**–**6**.

	1	**2**	**3**	**4**	**5**	**6**
Empirical formula	$C_{19}H_{17}N_3O_2$	$C_{18}H_{14}ClN_3O_2$	$C_{18}H_{13}Cl_2N_3O_2$	$C_{18}H_{13}Cl_2N_3O_2$	$C_{18}H_{15}N_3O_2$	$C_{19}H_{17}N_3O_2$
Formula weight	319.36	339.77	374.21	374.21	305.33	319.36
Crystal system	Monoclinic	Monoclinic	Orthorhombic	Triclinic	Orthorhombic	Monoclinic
Space group	$P2_1/c$	$P2_1/c$	*Pbca*	$P\bar{1}$	*Pbca*	$P2_1/c$
Unit cell parameters						
a (Å)	8.1089(15)	7.2078(10)	11.699(3)	11.7174(4)	13.6856(3)	15.7968(2)
b (Å)	26.857(4)	14.4418(15)	11.568(4)	11.9012(4)	10.3389(3)	5.8142(1)
c (Å)	7.1988(16)	14.9765(15)	24.584(3)	13.6483(4)	20.8395(6)	18.6854(3)
α (°)				94.461(2)		
β (°)	94.35(4)	98.973(10)		112.577(1)		115.860(1)
γ (°)				104.891(2)		
V (Å^3)	1563.3(5)	1539.9(3)	3326.8(1)	1664.86(9)	2948.67(14)	1544.32(4)
Z	4	4	8	4	8	4
D_{calc} (g cm^{-3})	1.357	1.466	1.494	1.493	1.376	1.374
F(000)	672	704	1536	768	1280	672
Cell parameters from	25 reflections	25 reflections	25 reflections	3538 reflections	4970 reflections	6619 reflections
θ range for lattice parameters (°)	18.86–37.60	18.77–35.51	20.33–34.66	3.58–65.18	4.24–66.72	3.11–68.53
Absorption coefficient μ (mm^{-1})	0.728	2.336	3.663	3.660	0.747	0.737
Absorption correction	Refdelf [11]	Multi-scan [12]	Refdelf	Multi-scan	Multi-scan	Multi-scan
T_{min}/T_{max}	0.619/0.804	0.442/0.663	0.435/0.693	0.581/0.756	0.8575/0.9996	0.712/0.988
θ range for data collection (°)	0.619/0.804	4.28–80.32	3.60–80.47	3.92–65.08	4.2–67.6	3.11–66.60
Index ranges h, k, l	0/10, −34/0, −9/9	−8/9, −1/18, −1/19	0/14, −14/0, 0/31	−13/13,−13/13,−16/16	−16/14, −11/12,−24/25	−18/18, −6/5, −21/21
No. of measured reflections	3576	3959	3633	17,583	26,210	13,830
No. of independent reflections	3347 (R_{int} = 0.048)	3323 (R_{int} = 0.016)	3633 (R_{int} = 0.000)	5273 (R_{int} = 0.063)	2641 (R_{int} = 0.054)	2679 (R_{int} = 0.032)
No. of observed reflections	2982 with $I > 2\sigma(I)$	2928 with $I > 2\sigma(I)$	2706 with $I > 2\sigma(I)$	4044 with $I > 2\sigma(I)$	2171 with $I > 2\sigma(I)$	2419 with $I > 2\sigma(I)$
Refinement method			*Full-matrix least-squares on F^2*			
Final R indices: R, $wR(F^2)$	0.052,0.137	0.046, 0.128	0.070, 0.207	0.052, 0.138	0.0384, 0.0982	0.035, 0.095
Goodness-of-fit on F^2, S	1.037	1.075	1.111	1.049	1.037	1.036
Data/parameters	3347/268	3323/260	3633/229	5273/457	2641/212	2679/221
Extinction coefficient	None	0.0082(7)	None	None	0.00053(8)	0.0033(4)
Largest diff. peak and hole (eÅ^{-3})	+0.363/−0.298	+0.474/−0.441	+0.631/−0.497	+0.308/−0.437	+0.164/−0.127	+0.179/−0.134
$(\Delta/\sigma)_{max}$	0.000	0.001	0.000	0.000	0.000	0.001

Table 2
Selected bond lengths (Å) and angles (°) for **1**–**6**.

	1	**2**	**3**	**4**A	**4**B	**5**	**6**
N1—C21[a]	1.4251(17)	1.407(2)	1.418(3)	1.406(4)	1.403(4)	1.413(2)	1.4532(17)
N1—C2	1.3512(18)	1.360(2)	1.348(3)	1.367(4)	1.366(4)	1.3596(19)	1.3351(16)
C2—N3	1.3631(17)	1.356(2)	1.352(3)	1.357(3)	1.352(3)	1.3539(18)	1.3529(16)
C2—N6	1.3090(17)	1.309(2)	1.314(3)	1.301(3)	1.302(3)	1.3029(19)	1.3210(16)
C7—O10	1.3287(16)	1.332(2)	1.331(3)	1.325(3)	1.331(3)	1.3341(17)	1.3149(16)
C9—O11	1.2347(17)	1.239(2)	1.223(3)	1.244(3)	1.245(3)	1.2423(17)	1.2283(15)
C2—N1—C21[a]	125.63(11)	128.32(14)	125.1(2)	127.3(2)	128.1(2)	127.91(13)	126.01(11)
C2—N1—C5	110.14(11)	110.12(14)	111.3(2)	110.5(2)	110.2(2)	110.30(12)	110.47(11)
C5—N1—C21[a]	122.22(11)	121.36(15)	121.4(2)	122.1(2)	121.3(2)	121.72(13)	122.11(11)
C2—N1—C21—C22	145.47(15)	165.43(17)	−76.5(3)	−4.4(5)	−0.3(4)	−178.03(14)	–
C7—C8—C31—C32	−46.5(2)	−38.1(3)	−96.5(3)	49.9(4)	−42.4(4)	−42.7(2)	−116.02(14)
C2—N1—C12—C21	–	–	–	–	–	–	−98.93(15)
N1—C12—C21—C22	–	–	–	–	–	–	−22.27(17)

[a] N1—C12, C2—N1—C12 and C5—N1—C12 in **6**.

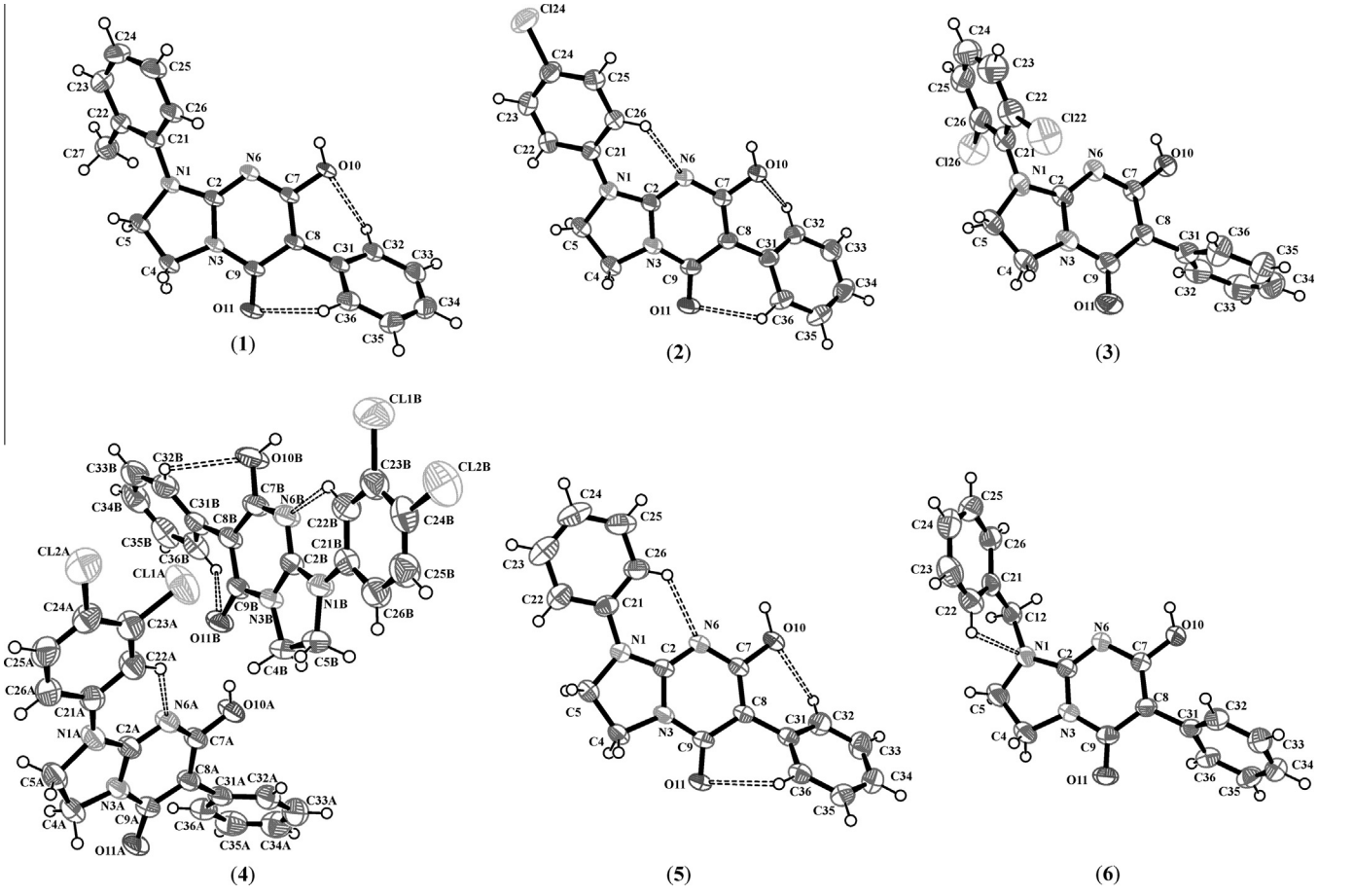

Fig. 1. A view of the molecules of compounds **1**–**6** in conformation observed in their crystals with the atom labeling scheme. Displacement ellipsoids are drawn at the 50% probability level.

SHELXS97 [10] and refined by full-matrix least-squares with SHELXL97 [10]. In **1** and **2** all hydrogen atoms were located by difference Fourier synthesis. For compounds **3**–**6** the O—bounded H atoms were located in $\Delta\rho$ maps and the remaining H atoms were positioned geometrically and treated as riding on their C atoms with C—H distances of 0.93 Å (aromatic), 0.97 Å (CH_2) and 0.96 Å (CH_3). All H atoms were refined with isotropic displacement parameters taken as 1.5 times those of the respective parent atoms. Crystal and experimental data of **1**–**6** are listed in Table 1. Molecular graphics were prepared using ORTEP3 for Windows [13]. PARST [14] and PLATON [15] were used for geometrical calculations. All calculations were performed using WINGX package [13].

Computational details

The theoretical calculations at the DFT/B3LYP level with 6-311++G(d,p) basis set implemented in GAUSSIAN 03 [16] were carried out to investigate the tautomeric equilibrium of **1**–**6** in gaseous phase and water, DMSO, methanol, n-octanol, chloroform and tetrachloromethane solutions (The Conductor Polarizable Continuum Model; CPCM [17]). The structures of all possible tautomeric forms were fully optimized without any constraint and the initial geometries were built from crystallographic data of **1**–**6**. The energy of each tautomeric form of **1**–**6** in solutions with CPCM model was calculated for geometry of respective molecule

Table 3
Hydrogen bonding geometry (Å, °) for **1–6**.

D—H···A	D—H	H···A	D···A	D—H···A	Symmetry codes
1					
C32—H321···O10	0.98(2)	2.56(2)	2.900(2)	100.1(16)	
C36—H361···O11	0.97(2)	2.53(2)	2.967(2)	107.1(17)	
O10—H101···O11^{i}	0.85(3)	1.84(3)	2.5992(16)	147(3)	*i* = *x*, *y*, 1 + *z*
2					
C26—H261···N6	0.98(3)	2.39(3)	2.988(2)	118.7(17)	
C32—H321···O10	0.95(3)	2.43(3)	2.849(2)	106.4(19)	
C36—H361···O11	1.01(3)	2.39(3)	2.936(3)	113.2(19)	
O10—H101···O11^{i}	0.85(3)	1.92(3)	2.6773(18)	147(3)	*i* = 1 + *x*, *y*, *z*
C22—H221···O11^{ii}	0.96(3)	2.49(3)	3.247(2)	136(2)	*ii* = 1−*x*, −1/2 + *y*,1/2−*z*
C26—H261···O10^{iii}	0.98(3)	2.59(3)	3.495(2)	153(2)	*iii* = 2−*x*, 2−*y*, −*z*
3					
O10—H101···N6^{i}	0.91(4)	1.84(3)	2.740(3)	170(5)	*i* = 1−*x*, 1−*y*, 1−*z*
4					
O10A—H10A···O11B	0.79(5)	1.86(5)	2.636(3)	165(6)	
C22A—H22A···N6A	0.93	2.23	2.878(4)	126	
C22B—H22B···N6B	0.93	2.25	2.891(4)	125	
C32B—H32B···O10B	0.93	2.51	2.892(4)	105	
C36B—H36B···O11B	0.93	2.55	2.952(4)	107	
O10B—H10B···O11A^{i}	0.96(5)	1.71(5)	2.644(3)	162(7)	*i* = *x*, *y*, 1 + *z*
C5A—H51A···O11B^{ii}	0.97	2.59	3.501(4)	157	*ii* = 1−*x*, 1−*y*, −*z*
C5B—H52B···O11A^{iii}	0.97	2.37	3.287(4)	158	*iii* = 1−*x*, 2−*y*, −*z*
5					
C26—H26···N6	0.93	2.25	2.892(2)	126	
C32—H32···O10	0.93	2.48	2.9052(19)	108	
C36—H36···O11	0.93	2.58	2.9777(18)	106	
O10—H10···O11^{i}	0.97(2)	1.72(2)	2.6737(15)	167.5(19)	*i* = 1/2 + *x*, *y*, 3/2−*z*
C5—H52···O11^{ii}	0.97	2.57	3.3311(18) 136	*ii* = 1−*x*, 1/2+*y*, 3/2−*z*	
6					
C22—H22···N1	0.93	2.60	2.908(2)	100	
O10—H10···N6^{i}	0.91(2)	1.87(2)	2.7626(16)	168(2)	*i* = −*x*, 1−*y*, 2−*z*
C12—H12B···O10^{i}	0.97	2.36	3.1839(18)	142	*i* = −*x*, 1−*y*, 2−*z*
C36—H36···O11^{ii}	0.93	2.40	3.3245(17)	171	*ii* = *x*, 1 + *y*, *z*

obtained in gaseous phase. Calculated energies in gaseous phase for all tautomeric forms were corrected for the zero-point energy (ZPE). The population analysis of tautomeric forms was estimated using non-degenerate Boltzmann distribution. The vibrational frequencies calculated for all possible tautomeric forms of **1–6** were scaled by 0.9679 for DFT/B3LYP/6-311++G(d,p) [18]. All experimental and calculated vibrational frequencies were compared for the model compound **5**, while for the other compounds this comparison was limited to the characteristic bands of OH and C=O groups. The calculated chemical shifts of the ^{1}H NMR and ^{13}C NMR spectra were obtained from the GIAO method [19,20] using TMS as reference. The visualization of theoretical calculation results was made using GaussView [21].

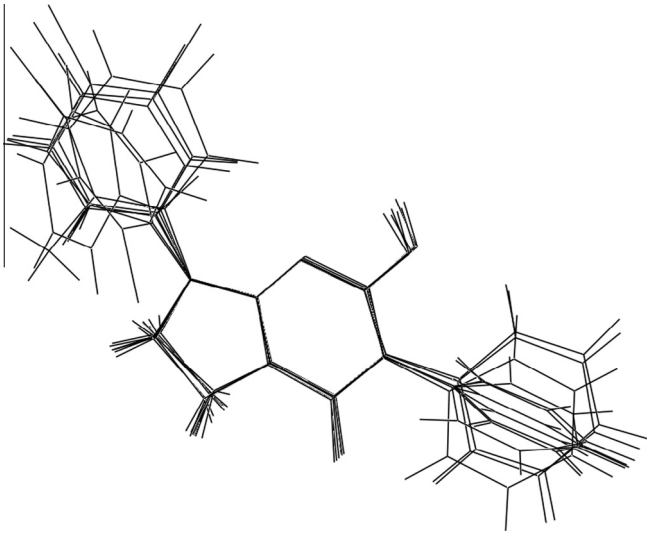

Fig. 2. Overlay of X-ray molecules of compounds **1–6** by least-squares fitting of the atoms of imidazopyrimidine rings (RMS = 0.0596 Å).

Results and discussion

Synthesis

The synthesis of compounds **1–6** is shown in Scheme 1. These compounds were obtained by condensation of the respective 1-aryl-4,5-dihydro-1*H*-imidazol-2-amine hydrobromide and diethyl phenylmalonate in presence of sodium methoxide in methanol [8]. The synthesized compounds **1–6** were characterized by elemental analysis, IR, ^{1}H and ^{13}C NMR, as well as X-ray analysis.

Spectroscopic analysis

The spectroscopic studies ^{1}H and ^{13}C NMR performed for compounds **1–6** confirmed their structure, but they do not allowed to explicitly indicate the tautomeric forms present in solution. In the ^{1}H NMR spectra of investigated compounds broadened resonance signals are observed, which may indicate a high rate of proton exchange processes between the different tautomeric forms, so only the "average" spectrum can be recorded. The process of proton exchange is fast in the time scale of the NMR experiment and it does not allow for a classical one-dimensional NMR spectra unambiguously identify the tautomeric forms present in solution. Moreover, the protons bonded to heteroatoms may be involved in hydrogen bonds. Increasing the strength of such hydrogen bond

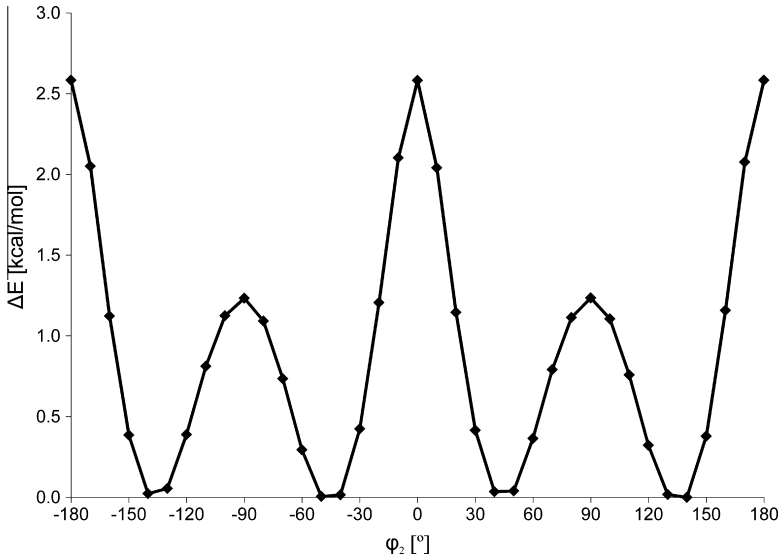

Fig. 3. The energy effect of the free-rotation between the phenyl ring and imidazo[1,2-*a*]pyrimidine system (C8—C31, φ_2) for the molecule **4** calculated using DFT/B3LYP/6-311++G(d,p) method.

results in a reduction of the electron density around a proton and resonance signal is shifted toward higher frequencies. The characteristic chemical shifts of OH groups in compounds **1**–**6** vary within the range of 10.90–11.22 ppm. ^{1}H NMR spectra exclude tautomeric form (***c***), because the hydrogen atom attached to the carbon atom C6 cannot resonate in this range. ^{13}C NMR spectra also did not allow to establish the tautomeric equilibrium, due to high similarity of surroundings of carbon atoms in the tautomeric forms of **1**–**6**. The chemical shifts for the C atom with a hydroxyl and carbonyl groups being in the ranges of 160.8–162.0 and 161.1–170.4 ppm, respectively, exclude tautomeric form (***c***), while forms (***a***) and (***b***) appear to be equally probable and can coexist in the solution.

The IR spectra were performed in solid state (KBr) for all investigated compounds **1**–**6** and chloroform solution for **4**. IR spectra in KBr show the characteristic narrow absorption bands in the range 1668–1632 cm^{-1} corresponding to the stretching vibration of the carbonyl group for a fused imidazopyrimidine system. The broad absorption band characteristic of the hydroxyl group present in the range 3435–3171 cm^{-1} confirms the possibility of the formation of hydrogen bonds. These observations allow to conclude that in the solid phase all forms (***a***)–(***c***) of **1**–**6** can occur. IR spectrum recorded in the solvent ($CHCl_3$) for compound **4** does not reveal a stretching vibration characteristic for the hydroxyl group, which may indicate a potentially existence diketo form (***c***) in solution.

Spectroscopic studies ^{1}H, ^{13}C NMR and IR, although allowed for the identification of the compounds **1**–**6** but they did not indicate explicitly their tautomeric forms present in solution and in the solid state. Therefore, for a full analysis of tautomeric equilibria a simulation of NMR and IR spectra using theoretical calculation were performed, in order to compare them with the experimental data.

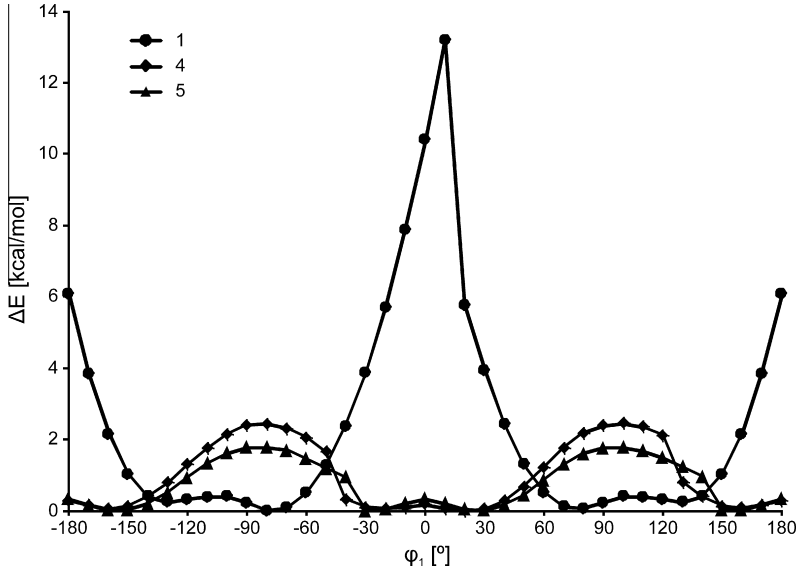

Fig. 4. The energy effect of the free-rotation between the phenyl ring and imidazo[1,2-*a*]pyrimidine system (N1—C21, φ_1) for the molecules **1**, **4** and **5** calculated using DFT/B3LYP/6-311++G(d,p) method.

X-ray investigations

Selected geometrical parameters for the X-ray investigated crystal structures of (**1**)–(**6**) are summarized in Table 2. The X-ray structure analysis of **4** revealed, that the asymmetric part of the unit cell contains two independent molecules A and B. View of the molecules with numbering of the atoms is shown in Fig. 1.

Difference electron-density maps for **1**–**6** revealed the position of the H atom in the vicinity of atom O10 with the bond lengths for C7—O10 and C9—O11 (Table 2) comparable with those for hydroxyl and carbonyl groups, respectively, clearly indicating that all molecules exist as the O10-enol/O11-keto (***a***) tautomeric form in the crystalline state. It is worth emphasizing that the hydroxyl and carbonyl groups in **1**, **2**, **4** and **5** are involved in a strong intermolecular O10—H101···O11 (Table 3) hydrogen bond.

The bond lengths and angles in the imidazopyrimidine system are very similar in **1**–**6** and close related structures of 6-benzyl-7-hydroxy-1-(2-methoxyphenyl)-2,3-dihydro-1*H*,7*H*-imidazo[1,2-*a*]pyrimidin-5(1*H*)-one [22] and 6-(2-chlorobenzyl)-1-(4-chlorophenyl)-7-hydroxy-2,3-dihydro-1*H*-imidazo[1,2-*a*]pyrimidin-5(1*H*)-one [23]. The aromatic pyrimidine rings are planar to within 0.053(16) Å in **1**, 0.0354(17) Å in **2**, 0.013(2) Å in **3**, 0.028(3) and 0.032(3) Å in molecules A and B of **4**, respectively, 0.0355(15) Å in **5** and 0.0165(12) Å in **6**. In **1**, **2** and **6**, the partially saturated imidazoline rings exist in an intermediate conformation between sofa and half-chair with respective characteristic asymmetry parameters [24] for these conformations of $\Delta C_s^{C4} = 2.64(19)^\circ$ and $\Delta C_2^{C2} = 2.31(19)^\circ$ in **1**, $\Delta C_s^{C5} = 4.1(2)^\circ$ and $\Delta C_2^{C2} = 2.\ 1(2)^\circ$ in **2** and $\Delta C_s^{C5} = 3.50(16)^\circ$ and $\Delta C_2^{C2} = 2.48(16)^\circ$ in **6**, while in **3**, **4** and **5** the imidazoline rings are nearly planar to within 0.016(2) Å in **3**, 0.003(3) and 0.0015(4) Å in molecules A and B of **4**, respectively and 0.0209(6) Å in **5**.

The orientation of the 1-(un)substitutedphenyl substituent in relation to the imidazo[1,2-*a*]pyrimidine system in **1**–**5**, as shown by the torsion angle φ_1 = C2—N1—C21—C22 of 145.47(15)° in **1**, 165.44(17)° in **2**, −76.5(3)° in **3**, −4.4(5) and −0.3(4)° in molecule A and B of **4**, respectively, −178.03(14)° in **5**, is strongly influenced by the steric effect of respective 2-methyl, 4-chloro, 2,5-dichloro and 3,4-dichloro substituents in phenyl ring. The orientation of the phenyl substituent at C8 position of the imidazopyrimidine ring changes from *gauche* for **1**, **2**, **4**, **5** and **6** to nearly perpendicular for **3**, as evidenced by the torsion angle φ_2 = C7—C8—C31—C32 of −46.5(2) for **1**, −38.1(3) for **2**, 49.9(4) and −42.4(4)° for A and B of **4**, respectively, −42.7(2)° for **5**, 65.19(18)° for **6** and −96.5(3)° for **3**. The weak intramolecular C—H···N and C—H···O hydrogen bonds (Table 3) giving slightly puckered six-ring fused system for **1**, **2**, **5** and **4**B, and four-ring fused system for molecule **4**A can be probably responsible for the conformations of molecules **1**, **2**, **4** and **5**. In **6**, the benzyl substituent has a *gauche–trans* conformation with the torsion angles C2—N1—C12—C21 of −98.63(15)° and N1—C12—C21—C22 of −22.27(17)°. This position of the benzyl group with respect to the imidazo[2-*a*]pyrimidine system is stabilized by the intramolecular C22—H22···N1 hydrogen bond (Table 3). The differences between conformations of molecules **1**–**6** are illustrated in Fig. 2 showing the overlay of all molecules by fitting of pyrimidine rings.

The X-ray structure analysis of **4** showed, that the asymmetric part of the unit cell contains two independent molecules A and B. The conformations of these molecules described by the torsion angles φ_1 [−4.4(5)° in A and −0.3(4)° in B] and φ_2 [49.9(4)° in A and −42.4(4)° in B] differ significantly by a rotation of phenyl ring around C8—C31 bond by about 90°. The theoretical calculations at the DFT/B3LYP/6-311++G(d,p) level show that the conformation of molecules A and B as observed in their crystal are not equi-energetic, with a difference in energy between A and B conformation of ΔE = 30.423 kcal/mol (single-point energy calculations).

Table 4
The stabilization energy ΔE (kcal/mol) and population (p_i) for tautomeric forms for **1**–**6**.

Tautomeric form		Gaseous phase		DFT B3LYP 6-311++G(d,p)/CPCM*											
				Water		DMSO		Methanol		n-Octanol		Chloroform		CCl_4	
		ΔE	p_i	ΔE	p_i	ΔE	p_i	ΔE	p_i	ΔE	p_i	ΔE	p_i	ΔE	p_i
1	(***a***)	0	1.00	0	0.96	0	0.99	0	0.99	0	1.0	0	0.99	0	1.00
	(***b***)	12.9	0	10.7	0	10.8	0	8.6	0	12.6	0	11.7	0	12.4	0
	(***c***)	5.2	0	1.8	0.04	4.4	0.01	4.6	0.01	5.3	0	4.8	0.01	5.1	0
2	(***a***)	0	0.99	0	1.0	0	0.98	0	0.99	0	0.99	0	0.99	0	0.99
	(***b***)	11.9	0	10.6	0	8.5	0	10.6	0	9.2	0	11.2	0	11.5	0
	(***c***)	4.8	0.01	5.1	0	2.4	0.02	4.9	0.01	2.7	0.01	3.7	0.01	4.8	0.01
3	(***a***)	0	0.99	0	0.99	0	0.99	0	0.99	0	0.99	0	0.99	0	0.99
	(***b***)	13.0	0	10.5	0	10.9	0	10.7	0	10.9	0	11.7	0	12.4	0
	(***c***)	4.9	0.01	4.3	0.01	4.2	0.01	4.3	0.01	3.7	0.01	4.5	0.01	4.7	0.01
4	(***a***)	0	0.99	0	1.0	0	1.0	0	1.0	0	0.99	0	1.0	0	1.0
	(***b***)	11.6	0	10.4	0	10.5	0	10.6	0	10.4	0	11.0	0	11.2	0
	(***c***)	4.9	0.01	5.7	0	5.4	0	5.6	0	4.9	0.01	5.4	0	5.1	0
5	(***a***)	0	0.99	0	1.0	0	0.99	0	1.0	0	0.99	0	0.99	0	0.99
	(***b***)	12.3	0	10.6	0	10.8	0	10.8	0	10.7	0	11.5	0	11.8	0
	(***c***)	4.9	0.01	5.1	0	4.9	0.01	5.1	0	4.6	0.01	5.0	0.01	4.9	0.01
6	(***a***)	0	0.99	0	0.99	0	0.99	0	0.99	0	0.99	0	0.99	0	0.99
	(***b***)	12.4	0	11.3	0	11.9	0	11.6	0	12.2	0	12.3	0	12.9	0
	(***c***)	4.0	0.01	3.5	0.01	3.7	0.01	3.6	0.01	4.0	0.01	3.9	0.01	4.4	0.01

* CPCM – The Conductor Polarizable Continuum Model.

However, the energy minimization and full geometry optimization with initial geometries obtained from the X-ray analysis for molecules A and B yielded a very small difference in energy of 0.012 kcal/mol between the conformations of molecule A ($\varphi_1 = -21.6°$ and $\varphi_2 = 44.6°$) and B ($\varphi_1 = -22.7°$ and $\varphi_2 = -45.6°$) without changing significantly the conformations of these molecules in relation to the conformations observed in crystal. Therefore the energy effect of the free-rotation between the phenyl ring and imidazo[1,2-*a*]pyrimidine system, taking into account the one degree of freedom described by the torsion angle φ_2, were calculated using DFT/B3LYP/6-311++G(d,p) method. The energies of conformations were minimized and all geometrical parameters optimized for each rotation with a 10° increment from −180 to 180° of φ_2 (Fig. 3). The conformations of molecules A and B observed in the crystalline state are in good agreement with calculated conformations with minima of energy for φ_2 of −50° and +50°. These two minima, similarly as two other minima at $\varphi_2 = -130°$ and +130°, are separated by the energy barrier estimated to about 2.7 kcal/mol for the phenyl ring to pass through mutual parallel position with pyrimidine ring ($\varphi_2 = 0°$ and ±180°). The presented value of energy shows that the molecule **4** can rotate freely about C8—C31 bond in the room temperature. The same can be concluded for molecules **1**, **2**, **3**, **5** and **6** noting that their conformations in crystal described by torsion angle φ_2 are very close to the conformations corresponding the calculated minima of energy for molecule **4**. The similar conformational analysis performed for torsion angle φ_1 for compounds **1**, **4** and **5** (Fig. 4) shows, that the position of the phenyl substituent with respect to the imidazo[1,2-*a*]pyrimidine system and the energy value of the rotation barrier are related with the type and place of the substituent in the benzene ring. The calculated energy minima for φ_1 are in good agreement with the value of φ_1 observed in the crystals of compounds **1**, **4** and **5**.

The molecular packing in the crystals of **1**–**6** is presented in Figs. S1–S6 in Supplementary Materials. In the crystal structure of **1** the strong intermolecular O10—H101···O11 hydrogen bond links the translation-related molecules into chains along the [0 0 1] direction. In the crystal structure of **2** the inversion-related molecules form dimers *via* pair of the C26—H261···O10 hydrogen bonds. Similarly as in **1**, the strong O10—H101···O11 resonance-assisted hydrogen bond links translation-related molecules into molecular chains along the [1 0 0] direction. Additionally, the molecules related by the 2_1 symmetry axis are joined in molecular chains parallel to the [0 1 0] direction by a weak C22—H221···O11 hydrogen bond. These two last intermolecular hydrogen bonds links the dimers in molecular layers parallel to the (0 0 1) crystallographic plane. Pairs of the pyrimidine rings belonging to inversion-related molecules partially overlap, with the $\pi\cdots\pi^{(i)}$ distance of 3.6594(6) Å; symmetry code: $(i) = 1-x, 2-y, -z$ and slippage of 1.637 Å. In the crystal structure of **3** the molecules related by centre of inversion form dimers through strong O10—H101···N6 hydrogen bond. In the crystal structure of **4** the pairs of hydrogen bonding molecules A and B from asymmetric part of the unit cell form molecular chains along *c* axis by the O10A—H10A···O11B and O10B—H10B···O11A strong resonance-assisted hydrogen bonds. These molecular chins are linked in three-dimensional network through the weak C5A—H51A···O11B and C5B—H52B···O11A hydrogen bonds. Additionally, the pyrimidine and C21···C26 benzene rings in inversion-related molecules A and inversion-related molecules B overlap each other in head-to-tail orientation. The $\pi\cdots\pi$ distances in the pair of molecules A are 3.3933(11) Å between pyrimidine/benzene $(1-x, 1-y, -z)$ and 3.5181(14) Å between benzene/pyrimidine $(1-x, 1-y, -z)$ rings. Corresponding $\pi\cdots\pi$ distances for overlapping molecules B in (x, y, z) and $(1-x, 2-y, 1-z)$ positions are 3.4005(13) and 3.4900(17) Å, respectively. In the crystal structure of **5**, molecules related by the *a* glide plane and 2_1 symmetry axis are linked into chains parallel to [1 0 0] and [0 1 0] direction *via* strong O10—H10···O11 and weak C5—H52···O11 intermolecular hydrogen bonds, respectively. The combinations of the [1 0 0] and [0 1 0] chains gives hydrogen-bonded molecular layers in the (0 0 1) crystallographic plane. The π-electron systems of the pairs of pyrimidine and benzene rings belonging to the molecules related by *c* glide plane overlap each other, with centroid-to-centroid separation of 3.6447(9) Å between pyrimidine ring at (x, y, z) and benzene ring at $(1/2-x, 1/2+y, z)$ and benzene ring at (x, y, z) and pyrimidine ring at $(1/2-x, -1/2+y, z)$. The $\pi\cdots\pi$ distances are 3.5284(5) and 3.4743(7) Å, respectively, and the angle between overlapping planes is 7.52(8)°. In the crystal structure of **6** the dimers formed from inversion-related molecules by two pairs of O10—H10···N6 and C12—H12B···O10 hydrogen bonds are linked into molecular chains along *b* axis by weak C32—H32···O11 hydrogen bond. It is noticeable, that in the all analyzed crystal structures the numerous weak C—H···π intermolecular contacts are observed (Table S1 in Supplementary Materials).

The molecular packing in the crystals of investigated compounds is determined by intermolecular hydrogen bonds, C—H···π, $\pi\cdots\pi$ and van der Waals interactions. A special role is played by a strong O—H···O and O—H···N intermolecular hydrogen bonds, which on one hand stem from the tautomeric form, and on the other hand affects the occurrence of well-defined tautomeric forms in the crystals of investigated compounds.

Theoretical calculations

In order to find the relative stabilities of the tautomeric forms of analyzed 1,6-aryl-7-hydroxy-2,3-dihydroimidazo[1,2-*a*]pyrimidin-5(1*H*)-ones, energy calculations for each of the three possible tautomeric forms of compounds **1**–**6** were performed in the gas phase and water, DMSO, methanol, n-octanol, chloroform and tetrachloromethane solutions using DFT method. The stabilization energy for each tautomeric form, expressed as the energy difference between the energy of given tautomeric form and the energy

Table 5
Comparison of experimental (E) and theoretical (T_{sc}) characteristic stretching bands ν (cm^{-1}) of the OH and C=O groups in the tautomeric forms (***a***)–(***c***) of compounds **1**–**6**.

Tautomer	E	T_{sc}			E	T_{sc}			E	T_{sc}		
		a	***b***	***c***		***a***	***b***	***c***		***a***	***b***	***c***
Compound	**1**				**2**				**3**			
ν OH	3171	3660	3602	–	3431	3669	3602	–	3435	3662	3602	–
ν C=O	1640	1665	1673	1721	1660	1668	1674	1724	1668	1667	1678	1726
				1694				1698				1699
Compound	**4**				**5**				**6**			
ν OH	3434	3669	3602	–	3430	3665	3602	–	3435	3664	3602	–
ν C=O	1637	1670	1675	1726	1632	1666	1672	1722	1652	1666	1672	1720
				1700				1685				1694

T_{sc} – Theoretical oscillation frequency scaled by a literature scaling factor 0.9679.

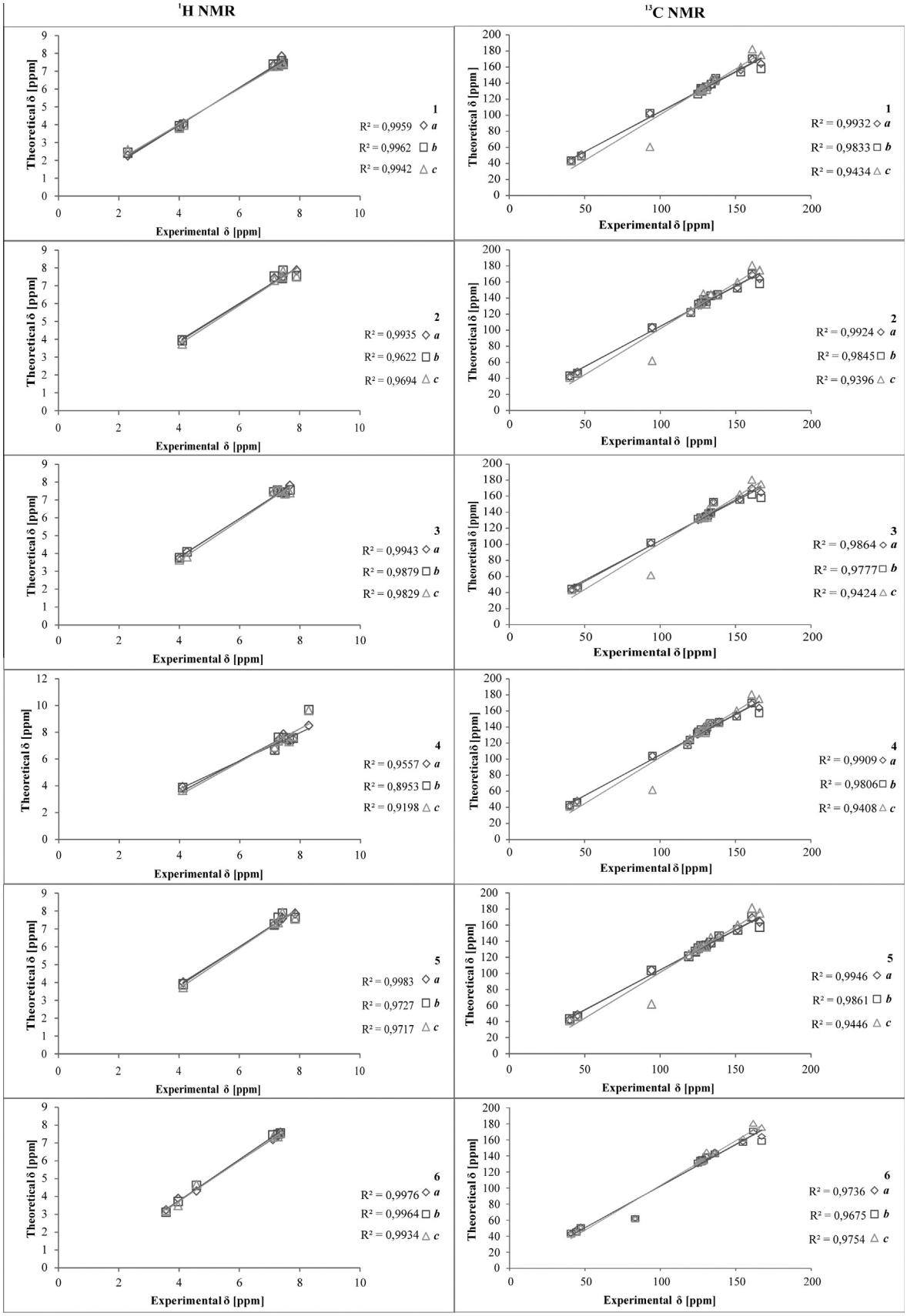

Fig. 5. The linear regression of experimental and calculated (GIAO DFT/B3LYP/6-311++G(d,p) method) chemical shifts in ^{1}H (column left) and ^{13}C (column right) NMR spectra for **1**–**6**. The signals derived from the protons of the hydroxyl group and methine atom C8 are omitted.

of the tautomeric form with lowest energy, was calculated and the population (fractional participation), p_i, of each form in the tautomeric form distribution was estimated using a non-generate Boltzmann distribution. The results of these calculations are presented in Table 4. As can be seen from Table 4, the population of the tautomeric form (***b***) in considered environments is below the threshold of the detectability of conventional analytical methods with the stabilization energy within the range from 8.5 to 13.0 kcal/mol for **2** in DMSO solution and **3** in gaseous phase, respectively. The other two tautomeric forma (***a***) and (***c***) can coexist both in gas phase and the solution, wherein the population of them is according with the relation (***a***) > (or ≫) (***c***). Influence of solvent polarity on tautomeric equilibrium is negligible resulting in changes in the population forms within a few percent and an explicit relationship between population form and the polarity of the solvent is not observed. Nevertheless one can see that the population of the form (***c***) for **1**, **2** and **6** increased slightly with the polarity of the solvent and an inverse relationship can be observed for form (***c***) in **4** and **5**. The results of the theoretical calculations of tautomeric equilibrium in gaseous phase and solutions for **1**–**6** are in good agreement with the experimental data obtained for these compounds in crystalline state. Although, the tautomeric form O10-oxo/O11-hydroxy (***a***), and form O10-oxo/O11-oxo (***c***), can be observed in gaseous phase and solutions and only tautomeric form (***a***) is observed in crystalline state, but due to proton-acceptor character of both oxo groups in tautomeric form (***c***), the lack of intermolecular O—H···O hydrogen bonds can be an important factor destabilizing the structure of the potential crystal of form (***c***).

Theoretical IR spectra calculated for possible tautomeric forms of **1**–**6** using DFT/B3LYP/6-311++G(d,p) method were compared with the experimental spectra recorded in KBr for these compounds. Since the calculated "raw" spectra usually significantly overestimate harmonic frequencies in comparison to experimental values, the scaling method was applied to best fit calculated and experimentally determined vibrational frequencies. Calculated vibrational frequencies were scaled by the scaling factor of 0.9679 recommended for the method and the basis set used in theoretical calculation [18].

As noted above (Part 3.2) the IR spectra recorded in KBr for all investigated compounds show the bands characteristic for O—H and C=O groups occurring in the tautomeric forms (***a***)–(***c***). All experimental and calculated vibrational frequencies were compared for the model compound **5** (Table S2 and Fig. S7 in Supplementary Materials), while for all compounds **1**–**6** this comparison limited to the characteristic bands of the groups OH and C=O is shown in Table 5.

As can be seen in Tables 5 and S2, the comparison of the experimental with theoretically calculated vibrational frequencies gave a difference of several cm^{-1} in $\Delta\nu$ for all tautomeric forms (***a***)–(***c***). The great similarity in the oscillation frequencies of both hydroxy and carbonyl groups at various positions **5** and **7** of the imidazo[1,2-*a*]pyrimidine ring confirms the difficulty in distinguishing three tautomers (***a***), (***b***) and (***c***) using IR spectra.

Although NMR spectroscopy is a widely used experimental method for structural analysis of organic compounds, it encounters a series of interpretation difficulties, particularly in the analysis of polyatomic molecules that can also exist as various tautomeric or isomeric forms. In such cases, it happens that the experimental spectrum does not give a full and explicit analysis of the structure of these compounds. However, the NMR spectra obtained from theoretical calculation allow the unambiguous assignment of signals from individual nuclei of atoms, and comparing it with the experimental spectrum can confirm or rule out the existence of various forms of the investigated compounds.

All experimental and theoretical calculated ^{1}H and ^{13}C NMR chemical shifts for compounds **1**–**6** are presented in Table S3 (Supplementary Materials; atoms numbers used for GIAO-DFT calculations are shown in Scheme S1). Comparison of experimental and calculated ^{1}H NMR and ^{13}C NMR spectra for compound 5 are shown in Figs. S8 and S9, respectively (Supplementary Materials). The comparison of the ^{13}C NMR spectra for compounds **1**–**6** obtained from theoretical calculation with those recorded experimentally (Fig. 5) gave a good fit factors, for which the values of R^2 are in the ranges 0.9946–0.9736, 0.9861–0.9675 and 0.9754–0.9396 for tautomeric forms (***a***), (***b***) and (***c***), respectively. This indicates a slightly better fit ^{13}C NMR spectra for oxo-hydroxy tautomeric forms (***a***) and (***b***) in relation to the spectrum for dioxo form (***c***). Also calculated and experimentally recorded chemical shifts of all protons in ^{1}H NMR spectra for **1**–**6** show very good correlation (Fig. 4), except chemical shifts for the proton of the hydroxy group in tautomeric forms (***a***) and (***b***) and the proton of the methine C(8)H group in tautomeric form (***c***), which differences between theoretical and experimental values are within the range 5.01–6.76 and 6.52–6.84 ppm, respectively. This discrepancy between experimental and theoretical shifts is caused by the incapacity of polarizable continuum model in calculations of NMR spectra for systems with hydrogen bonds between solute and solvent. Omitting these protons, the values of correlation coefficients R^2 vary from 0.9983 to 0.9557 for tautomeric form (***a***), from 0.9964 to 0.8953 for tautomeric form (***b***) and from 0.9958 to 0.9198 for tautomeric form (***c***). The best fit of the experimental and theoretical ^{1}H NMR spectra is observed for tautomeric form (***a***) of compounds **2**–**5** and tautomeric form (***b***) of compound **1**. In practice, slight differences in the values of R^2 for tautomeric forms (***a***), (***b***) and (***c***) are not capable of identifying tautomeric forms based on their NMR spectra in the set of investigated compounds **1**–**6**. It should be noted that the inclusion of protons of groups —OH and C(8)H in correlation analysis give the correlation coefficients R^2 less than 0.32, which means that the chemical shifts of theoretical and experimental spectra are uncorrelated.

Conclusion

In this paper, the structural characterization of a series of imidazo[1,2-*a*]pyrimidine derivatives **1**–**6** with antinociceptive activity is reported. The compounds **1**–**6** can exist in three tautomeric forms and the tautomeric equilibrium between them in gaseous phase, solution and crystalline state was examined using IR, ^{1}H and ^{13}C NMR spectroscopic analysis, X-ray crystal structure determinations and theoretical calculations at DFT Level. The correlation analysis of the experimentally recorded IR, ^{1}H and ^{13}C spectra and the corresponding spectra theoretically calculated for all possible tautomeric forms of **1**–**6** show limited possibilities of use of these methods to identify their tautomeric forms in different environments. This may be due to the fact, that polarisable continuum model PCPM used for theoretical calculation may fail in describing the properties of systems with hydrogen bonds between solute and solvent. The obtained results of the structural investigation of compounds **1**–**6** may be helpful in the study of relations between chemical structure and biological activity (SAR and QSAR analysis) of the analyzed bioactive imidazo[1,2-*a*]pyrimidine.

Appendix A. Supplementary material

CCDC-1038738 for **1**, CCDC-1038739 for **2**, CCDC-1038740 for **3**, CCDC-1038741 for **4**, CCDC-1038742 for **5** and CCDC-1038743 for **6** contain the supplementary crystallographic data for this paper. These data can be obtained free of charge at www.ccdc.cam.ac.uk/conts/retrieving.html [or from the Cambridge Crystallographic Data Centre (CCDC), 12 Union Road, Cambridge CB2 1EZ, UK; fax: +44(0) 1223 336 033; email: deposit@ccdc.cam.ac.uk].

The weak C—H$\cdots\pi$ intermolecular contacts geometry for **1**–**6** (Table S1). The comparison of experimental and calculated stretching and bending vibrational frequencies in the IR spectra of the tautomeric forms (***a***)–(***c***) of the model compound **5** (Table S2). Experimental and calculated ^{1}H and ^{13}C NMR chemical shifts for compounds **1**–**6** (Table S3). Unit-cell packing in crystals of **1**–**6** (Fig. S1–S6). Comparison of experimental and calculated IR spectra for compound **5** (Fig. S7). Comparison of experimental and calculated ^{1}H NMR spectra for compound **5** (Fig. S8). Comparison of experimental and calculated ^{13}C NMR spectra for compound **5** (Fig. S9). Atom numbers used for GIAO calculation of ^{1}H and ^{13}C NMR chemical shifts (Scheme S1).

Supplementary data associated with this article can be found, in the online version, at http://dx.doi.org/10.1016/j.molstruc.2015.04.005.

References

[1] A.Sh. Oganisyan, A.S. Noravyan, I.A. Dzhagatspanyan, I.M. Nazaryan, A.G. Akopyan, Pharm. J. Chem. 41 (2009) 588.
[2] A.A. Abdel-Hafez, Arch. Pharm. Res. 30 (2007) 678.
[3] J.P. Zhou, Y.W. Ding, H.B. Zhang, L. Xu, Y.Y. Dai, Chem. Lett. 19 (2008) 669.
[4] F. Qi, J.-P. Zhou, Y.-W. Ding, W.-L. Huang, H. Qian, Y. Dai, J. China Pharm. Univ. 40 (2009) 16.
[5] O. Algul, A. Meric, S. Polat, N.D. Yuksek, M.S. Serin, Cent. Eur. J. Chem. 7 (2009) 337.
[6] D. Matosiuk, S. Fidecka, L. Antkiewicz-Michaluk, I. Dybała, A.E. Kozioł, Eur. J. Med. Chem. 37 (2002) 845.
[7] D. Matosiuk, S. Fidecka, L. Antkiewicz-Michaluk, J. Lipkowski, I. Dybała, A.E. Kozioł, Eur. J. Med. Chem. 37 (2002) 761.
[8] M. Rządkowska, E. Szacoń, A.A. Kaczor, S. Fidecka, E. Kędzierska, D. Matosiuk, Med. Chem. 10 (2014) 460.
[9] K. Sztanke, S. Fidecka, E. Kędzierska, Z. Karczmarzyk, K. Pihlaja, D. Matosiuk, Eur. J. Med. Chem. 40 (2005) 127.
[10] G.M. Sheldrick, Acta Cryst. A64 (2008) 112.
[11] S. Parkin, B. Moezzi, H. Hope, J. Appl. Cryst. 28 (1995) 53.
[12] Bruker, SADABS, Bruker AXS Inc., Madison, Wisconsin, USA, 2005.
[13] L.J. Farrugia, J. Appl. Cryst. 32 (2012) 849.
[14] M. Nardelli, Compd. Chem. 7 (1983) 95.
[15] A.L. Spek, J. Appl. Cryst. 36 (2003) 7.
[16] M.J. Frisch, G.W. Trucks, H.B. Schlegel, G.E. Scuseria, M.A. Robb, J.R. Cheeseman, J.A. Montgomery, Jr., T. Vreven, K.N. Kudin, J.C. Burant, J.M. Millam, S.S. Iyengar, J. Tomasi, V. Barone, B. Mennucci, M. Cossi, G. Scalmani, N. Rega, G.A. Petersson, H. Nakatsuji, M. Hada, M. Ehara, K. Toyota, R. Fukuda, J. Hasegawa, M. Ishida, T. Nakajima, Y. Honda, O. Kitao, H. Nakai, M. Klene, X. Li, J.E. Knox, H.P. Hratchian, J.B. Cross, V. Bakken, C. Adamo, J. Jaramillo, R. Gomperts, R.E. Stratmann, O. Yazyev, A.J. Austin, R. Cammi, C. Pomelli, J.W. Ochterski, P.Y. Ayala, K. Morokuma, G.A. Voth, P. Salvador, J.J. Dannenberg, V.G. Zakrzewski, S. Dapprich, A.D. Daniels, M.C. Strain, O. Farkas, D.K. Malick, A.D. Rabuck, K. Raghavachari, J.B. Foresman, J.V. Ortiz, Q. Cui, A.G. Baboul, S. Clifford, J. Cioslowski, B.B. Stefanov, G. Liu, A. Liashenko, P. Piskorz, I. Komaromi, R.L. Martin, D.J. Fox, T. Keith, M.A. Al-Laham, C.Y. Peng, A. Nanayakkara, M. Challacombe, P.M. W. Gill, B. Johnson, W. Chen, M.W. Wong, C. Gonzalez, and J.A. Pople, Gaussian 03, Revision E.01, Gaussian Inc, Wallingford CT, 2004.
[17] M. Cossi, N. Rega, G. Scalmani, V. Barone, J. Comput. Chem. 24 (2003) 669.
[18] M.P. Andersson, P. Uvdal, J. Phys. Chem. A 109 (2005) 2937.
[19] R. Ditchfield, Mol. Phys. 8 (1974) 397.
[20] K. Wolinski, J.F. Hilton, P. Pulay, J. Am. Chem. Soc. 112 (1990) 8251.
[21] Æ. Frisch, R.D. Dennington II, T.A. Keith, J. Millam, A.B. Nielsen, A.J. Holder, J. Hiscocks, GaussView Reference (Version 4.0.) Gaussian Inc., Wallingford, USA, 2007.
[22] W. Wysocki, D. Matosiuk, Z. Karczmarzyk, M. Rządkowska, Z. Urbańczyk-Lipkowska, Acta Cryst. E62 (2006) o2548.
[23] W. Wysocki, D. Matosiuk, M. Rządkowska, Z. Karczmarzyk, Z. Urbańczyk-Lipkowska, P. Kalicki, Acta Cryst. E66 (2010) o2742.
[24] W.L. Duax, D.A. Norton, Atlas of Steroid Structure, vol. 1, Plenum, New York, 1975.